Cellulose nanofibrils and silver nanowires active coatings for the development of antibacterial packaging surfaces

Spieser, Hugo; Denneulin, Aurore; Deganello, Davide; Gethin, David; Koppolu, Rajesh; Bras, Julien

Published in:
Carbohydrate Polymers

DOI:
10.1016/j.carbpol.2020.116305

Published: 15/07/2020

Document Version
Accepted author manuscript

Document License
CC BY-NC-ND

Cellulose nanofibrils and silver nanowires active coatings for the development of antibacterial packaging surfaces

Hugo Spieser[a, b], Aurore Denneulin[a], Davide Deganello[b], David Gethin[b], Rajesh Koppolu[c], Julien Bras[a, d]

[a]*Univ. Grenoble Alpes, CNRS, Grenoble INP*, LGP2, F-38000 Grenoble, France*

[b]*College of Engineering, Swansea University, Bay Campus, Crymlyn Burrows, Swansea SA1 8EN, UK*

[c]*Laboratory of Natural Materials Technology, Åbo Akademi University, 20500 Turku, Finland*

[d]*IUF, 75000 Paris, France*

Corresponding author:
aurore.denneulin@grenoble-inp.fr
+33(0)4 76 82 69 28
Laboratory of Pulp and Paper Science and Graphic Arts
461, rue de la Papeterie
CS 10065
38402 Saint-Martin d'Hères – France

Abstract: An active ink composed of cellulose nanofibrils and silver nanowires was deposited on flexible and transparent polymer films using the bar coating process, achieving controlled thicknesses ranging from 200 nm up to 2 µm. For 350 nm thick coating on polyethylene terephthalate films, high transparency (75.6% transmittance) and strong reduction of bacterial growth equal to 89.3% and 100% was noted respectively against Gram-negative *Escherichia Coli* and Gram-positive *Staphylococcus Aureus* bacteria using AATCC contact active standard test. Retained antibacterial activity was found with films produced by reverse gravure roll-to-roll process, showing the promising capability of this antibacterial solution to be deployed industrially. Finally, the same ink was also deposited on polylactic acid substrate to investigate barrier properties: for 350 nm thick coating, a reduction of 49% of oxygen transmission rate (dry conditions) and 47% reduction of water vapor transmission rate was noted, proving the enhanced barrier properties of the coatings.

Keywords: cellulose nanofibrils, silver nanowires, transparent coatings, antibacterial activity, barrier properties, up-scaling

* Institute of Engineering Univ. Grenoble Alpes

1. Introduction

In a high consumption society, production and global movement of food products is considerable and increasing continuously (Food and Agriculture Organization of the United Nations, 2019). Food products are exposed to harsh conditions throughout all of the supply chain stages and packaging is today expected to meet more and more requirements. Recent innovation has focused on the development of active packaging, which refers to the ability of a package to respond to an external stimulus (Yildirim et al., 2018). Within this framework, active packaging aims at increasing the shelf-life of a product by optimizing the condition inside the package, thus improving food quality and reducing food waste.

Antimicrobial food packaging has been studied extensively over the past 20 years and aspires to reduce pathogenic contamination against bacteria, fungus or viruses (Sofi et al., 2018) with a preferred mode of action working by contact for consumer safety and environmental concern. (Kaur & Liu, 2016). Silver nanoparticles (Ag NPs) have recently attracted a lot of attention since they display strong antibacterial activity and can help fighting against the increasing antibiotic resistance in pathogens (Rai et al., 2012). It has been established that the antibacterial effect of Ag NPs is attributed to the nanoscale of the particles itself along with the continuous release of silver ions (Morones et al., 2005). The morphology of Ag NPs plays a major role on their antimicrobial activity: the smaller the nanoparticle (the higher surface area) the more active they are against bacteria (Carlson et al., 2008). The shape of the nanoparticle is also important and the antibacterial activity decreases on progression from pyramids, cubes, spheres, to wire-like shape (Hong et al., 2016; Pal et al., 2007). Different parameters also influence the antibacterial activity of Ag NPs such as surface charge, the presence of residual synthesis surfactants or capping agent, and Ag NPs crystallinity. (El Badawy et al., 2011; Kvítek et al., 2008; Smetana et al., 2008).

One way to use Ag NPs in packaging applications is to incorporate them into a nanocomposite to limit nanoparticle migration. Indeed, Ag NPs have been recognized as potentially hazardous for health as studies have focused on evaluating their toxicity against in vivo and in vitro studies. There is still a lack of information and knowledge concerning the global health hazard on human, but Ag NPs are suggested to be mainly dangerous by oral and inhalation adsorption into the human body and silver accumulation in different organs leading to specific malfunctions (Korani et al., 2015). The potent activity of Ag NPs is dependent on a lot of factors such as size, surface chemistry, shape, etc. and more research is needed to have a full overview of the toxicity of Ag NPs toward the human body. It then appears obvious that the leaching of Ag NPs in antibacterial composite for food packaging application is important parameter to address. Nanocellulose materials are biobased, biodegradable and biocompatible nanomaterials that are defined as cellulose particles with a nano-scale size for at least one of their dimensions. One of the established class of nanocellulose are cellulose nanofibrils (CNF) which come from the mechanical

fibrillation of pulp suspension (Herrick et al., 1983; Turbak et al., 1983). CNF have been of particular interest because they display interesting properties for packaging applications: high oxygen barrier property, vast chemical functionalization possibilities and good mechanical properties. CNF can be used either alone as a free standing film or as a coating on classic plastic packaging or paper substrates for its reinforcement properties (Afra et al., 2016; Fukuzumi et al., 2009; Rodionova et al., 2012) and also display good matrix properties that can be used successfully to immobilize nanoparticles.

Combinations of Ag NPs and nanocellulose composites have been investigated extensively by the scientific community (Xu et al., 2017) and different composite preparation techniques exist. In the most common in-situ synthesis methods, CNF serve as a template matrix for adsorption of silver salts, followed by in-situ chemical reduction (Uddin et al., 2017; Yu et al., 2019). Covalent bonding is another option ,yet to our knowledge, the only reported example comes from Ramaraju, Imae, & Destaye (2015), who reported the immobilization of Ag NPs stabilized with a dendrimer by covalently bonding the NH_2-terminated dendrimer on TEMPO-oxidized CNF. Finally, the physical mixing approach is just mixing separately produced components. To our knowledge, the only example of simple mixing of CNF materials with Ag NPs for antibacterial applications has been reported by Martins et al. (2012) who prepared CNF/Ag NPs composites based on a polyelectrostatic assembly for antibacterial coating on a paper substrate. Simple mixing is a straightforward easily up-scalable procedure, however immobilization of the Ag NPs on cellulose materials is relatively poor (Ilić et al., 2009), leading to reduced life-time of the system and possible non-desired release of Ag NPs.

This work presents the development of antibacterial packaging based on a combination of silver nanoparticles and nanocellulose materials. Indeed, based on the precedent literature review, it was then hypothesized that combining silver nanowires with cellulose nanofibrils could achieve easy-to-process systems that can be deposited on flexible substrate to achieve contact killing antibacterial mode of action along with improved barrier properties. In this study, the technical challenges were firstly to straightforwardly produce a transparent and antibacterial coating on plastic polymer sheets. Secondly the objectives were to prepare similar active coatings on biobased polymer sheets and to evaluate the enhancement of their barrier property. Finally, the challenge of preparing active surfaces with a roll-to-roll process for up-scaling purposes was addressed.

To tackle the three core challenges, a hybrid ink composed of TEMPO-oxidised cellulose nanofibrils and silver nanowires was firstly deposited on polyethylene terephthalate substrates using laboratory-scale bar coating process. Thickness and transparency of the coatings were investigated and they were tested against bacterial contamination. The same technique was used to deposit the active ink on bio-based polylactic acid sheets and the barrier properties of the produced films were characterized. Finally, a new lower cost

active ink was specifically formulated by the authors to assess the up-scaling possibility by using a reverse gravure roll-to-roll coating process.

2. Materials and methods

2.1. Materials

A polyethylene terephthalate (PET) sheet substrate (Melinex® ST726 – 175 µm) and polylactic acid (PLA) substrate (Earthfirst® BCWC – 75 µm) was respectively purchased from Dupont (France) and Sidaplax (Belgium). A hybrid ink system composed of silver nanowires (Ag NWs) and TEMPO oxidised-cellulose nanofibrils (T-CNF) in water (PolyBioWire® 9830C) was supplied by Poly-Ink (France) with an approximate 1% wt total mass and 1:1 ratio given by the supplier. However to investigate a roll-to-roll semi-industrial deposition process, a new specific formulation was prepared, using T-CNF suspension (CNF-A13) from Betulium (Finland) with approximatively length of 50-400 nm and diameter of 5-15 nm, at 5 %wt (charge density of 1.6 ± 0.1 mmol.g^{-1}, estimated aspect ratio of 22.5) and using 2.5% wt Ag NWs aqueous suspension (NGAP NF Ag-3170) from NanoGap (USA) with estimated length 10-50 µm, diameter 50-100 nm (and so with an estimated aspect ratio of 400).

Escherichia Coli ATCC 8739 and Staphylococcus Aureus ATCC 6538 were purchased from Microbiologics (USA). PCA (Plate Counting Agar) was purchased from BD Difco (USA) and contains beef extract (3g.l^{-1}), peptone (5g.l^{-1}), agar (15g.l^{-1}). Standard nutrient broth 1 was purchased from Roth (Germany) and contains beef extract (3g.l^{-1}), peptone (15g.l^{-1}), sodium chloride (6 g.l^{-1}) and glucose (1g.l^{-1}). Sodium thiosulphate (>99%), L-histidine (>98.5%), potassium dihydrogen phosphate (>99%), Tween®80 and calcium chloride (>96%) were also obtained from Roth (Germany). L α-phosphatidyl choline (>99%) was purchased from Sigma Aldrich (France). All materials were used as received.

2.2. Active layer production by bar coating process

Coated films were first prepared using the supplied T-CNF/Ag NWs ink and bar coating process (KCC101, Erichsen, Germany). Prior to coating, the films were corona treated (Klwar Calvatron SG2, Germany): 2 passes, 90° rotation between the pass. The coatings were then oven-dried and different thickness were achieved using different threaded rod diameter (Supplementary data). Coatings, corona treatment and drying step parameters were optimized through extensive research with visual observation of possible defects, transparency and sheet resistance measurements. Optimized corona treatment settings are the following: 2.9 m.min^{-1} speed and 330 mA intensity for PET substrate, 3.5 m.min^{-1} speed and 150 mA intensity for PLA substrate. Optimized coatings and drying parameters are the following: coating speed of 5.4 m.min^{-1} for both PET and PLA coatings, oven-drying step at 120°C for 60s for PET and at

room temperature overnight for PLA coatings. Each coating was performed at least three times to assess consistency and reproducibility of the process.

2.3. Structural and quality characterization

Field-Emission Gun Scanning Electron Microscope (FEG-SEM) was used to investigate the hybrid nanostructure after 2 nm-coating of Gold /Palladium, at 5.4 mm working distance and 3 kV accelerating voltage. A cross-section through the coated samples was prepared using a LEICA UC6 (Germany) ultramicrotome apparatus equipped with a diamond knife, at room temperature and with a cutting speed of 1 $mm.s^{-1}$. The thickness of the coatings was then estimated by image analysis using FIJI software (Schindelin et al., 2012; Schneider et al., 2012). At least 6 measurements in three different positions in the films were considered.

Transmittance (%) was measured on a UV-spectrophotometer (Shimadzu Manufacturing Inc., USA), using the photometric mode. Six different measurements were conducted on each sample at 550 nm wavelength. Sheet resistance (Ω/sq) of the coated layer was measured by a four-probe system (Jandel Universal, USA). The measurement was repeated at six positions on the film and the average computed along with associated standard deviation.

2.4. Antibacterial characterization

Prior to antibacterial testing, a leaching assay was performed by putting a 2 x 2 cm specimen of coating (24 µm estimated wet thickness) in 10 ml of deionized water (DI), under agitation (100 rotation per minute) at 37°C. After 72 hours, the liquid media was recovered and full UV-vis spectra (300-700 nm wavelength, 1 nm scan rate) were recorded on a UV-spectrophotometer (Shimadzu Manufacturing Inc., USA), and compared with Ag NWs suspensions at 0.005% wt.

All the glassware, consumables, tools and solutions used for the antibacterial characterization were sterilized prior to use in autoclave for 20min at 120°C and 1.034 bar.

Antibacterial activity was assessed initially using an inhibition zone qualitative test following a modified AFNOR EN 1104 standard (AFNOR standard, 2005). To exaggerate the antibacterial activity of the samples, the test was carried out on multilayer coating (10 layers) prepared with the same parameters as single layer coating (threaded rod with 1.27 diameter –100 µm estimated wet thickness). Ag NWs only coating was used as control and prior to deposition, the starting suspension was diluted to 0.5% wt in DI and dispersed using an Ultra Turrax high shear disperser (30s, 10,000 rpm). The produced samples were cut into 5 cm x 5 cm specimens and dry-sterilized for 24 hours at 60°C. 10 ml of pre-inoculated PCA at

158 10^5 CFU.ml^{-1} (Colony Forming Unit) was poured in a petri dish and after cooling the samples were put on
159 top with the coated side facing the agar. The incubation period was 72 hours at 37°C and the inhibition
160 zone was assessed visually after incubation.

161 Quantitative tests were performed on single layer coatings with different thickness using a protocol
162 adapted from the AATCC TM100-1998 standard (AATCC standard, 1998). The samples were cut into 2
163 cm x 2 cm specimens and dry-sterilized for 24 hours at 60°C. 200 µl of bacterial suspension at 5.10^5
164 CFU.mL^{-1} in 20% nutrient broth (5 g.l^{-1} nutrient broth, 6.8 g.l^{-1} sodium chloride) were deposited on the
165 samples specimen and incubated at 37°C for 24 hours. After incubation, the bacterial suspension was
166 recovered by washing with a prepared neutralizing solution (3 g.l^{-1} of L-α-phosphatidyl choline, 5 g.l^{-1} of
167 sodium thiosulphate, 1 g.l^{-1} of L-histidine, 30 g.l^{-1} of Tween 80, 10 ml of potassium dihydrogen phosphate
168 at 0.0425 g.l^{-1}, controlled pH of 7.2 ± 0.2) and the final concentration was determined by the plate
169 counting numbering method. The antibacterial activity (AA, %) of the samples was compared
170 quantitatively using the following equation (1):

171 $$AA\ (\%) = \frac{BC_{reference} - \mathrm{BC}_{sample}}{BC_{reference}} \times 100 \qquad (1)$$

172 Where $\mathrm{BC}_{\mathrm{reference}}$ (log CFU) is the remaining bacterial concentration on the PET substrate with no coating
173 and $\mathrm{BC}_{\mathrm{sample}}$ (log CFU) is the remaining concentration on the tested sample.

174 **2.5. Barrier properties characterization**

175 The Oxygen Transmission Rate (OTR) of the coated samples was measured at 0, 50 and 80 % humidity
176 rate following the ASTM-F 1927-98 standards (ASTM standard, 2014) on a Systech Illinois Permeation
177 Analyser (USA) equipped with a coulometric detector. The tests were conducted at 23°C and with a 6.15
178 cm^{-1} exchange surface. At least 3 different samples for each coating were tested and an average is
179 computed along with the associated standard deviation.

180 Water Vapour Transmission Rate (WVTR) was also measured on the same samples following a slightly
181 modified T 448 om-09 standard (TAPPI Standard, 2009). Around 30 g of anhydrous calcium dichloride
182 salt was put in a metal cup covered by the test sample and closed by a rubber gasket and screw-down cap.
183 The test was conducted at a regulated temperature (23°C) and humidity (50 %). The water-uptake of the
184 anhydrous salt through the tested sample was monitored by weighing at least twice a day for at least one
185 week. The WVTR value was calculated using the following equation (2):

186 $$WVTR\ (g.m^{-2}.day^{-1}) = \frac{24 \times \Delta m}{\Delta t \times S} \qquad (2)$$

Where Δt (h) is the time between two measurements, Δm (g) the corresponding weigh-uptake and S (m^2) is the exposed surface (6.15 cm^2).

2.6. Specific ink formulation and characterization for up-scaling test

A specific, lower cost and in bigger volume formulation was prepared using T-CNF suspension (Betulium) and Ag NWs suspension (NanoGap) redispersed together at 1% wt total mass with a mass ratio of 1:1 using an Ultra Turrax high shear disperser (30s, 10,000 rpm).

T-CNF was imaged using a Philips CM 200/FEI (USA) Transmission Electron Microscope (TEM) equipped with a TemCam F216 from TVIPS (Germany), at 200 kV acceleration voltage. A diluted suspension of T-CNF was drop-casted on a copper grid with an amorphous carbon coating and uranyl acetate (2%) dye was deposited on the drop-casted sample. Ag NWs were imaged by Atomic Force Microscopy (AFM) and Scanning Electron Microscopy (SEM). AFM images were recorded on a Veeco NanoScope-V apparatus (Canada). Ag NWs suspension was drop-casted on a Mica susbtrate and dried overnight. A tapping mode with an OTESPA Bruker (USA) silicon cantilever was used covering a 3.3 µm x 3.3 µm surface area.

The sedimentation evolution of the formulated ink was characterized by putting 10 ml of ink into a cylindrical glass vial of 29 mm diameter section and measuring the sediment height after a fixed time. The sediment height (S, %) was calculated using the following equation (3):

$$S = \frac{H}{H_0} \times 100 \qquad (3)$$

Where H (mm) is the measured sediment height and H_0 (mm) the total liquid height.

The rheological studies were performed on a rotational rheometer (MCR02, Antonn Paar) at a set temperature of 20°C with a cone-plate geometry (1.013° angle, 50 mm diameter and 55 µm truncate) along with a set gap of 0.112 mm. Flow curves experiment were performed with increasing shear rate ranging from 0.1 to 1000 s^{-1}.

Reverse gravure coating was conducted using a Mini-Labo™ apparatus from MIRWEC Film, Inc./ Yasui Seiki company (USA). Coating was applied at a speed of 1 $m.min^{-1}$ and dried using infrared heaters. Two different coating weights were produced using two different gravure rolls: roll 30 (estimated surface volume of 150 $cm^3.m^{-2}$, estimated transfer fraction of 0.33 and estimated approximate wet coat thickness of 30-45 µm), and roll 120 (estimated surface volume of 34.7 $cm^3.m^{-2}$, estimated transfer fraction of 0.28 and estimated approximate wet coat thickness of 5-11 µm).

3. Results and discussion

3.1. Bar coating deposition on PET and antibacetrial properties.

The active ink was bar coated at 4 different thicknesses on PET sheets and the dry thickness was determined from a cross section captured by FEG-SEM imaging (Figure 1). For the thicker coatings the results demonstrated a higher standard deviation because the ultramicrotome cuts damaged the coated layer.

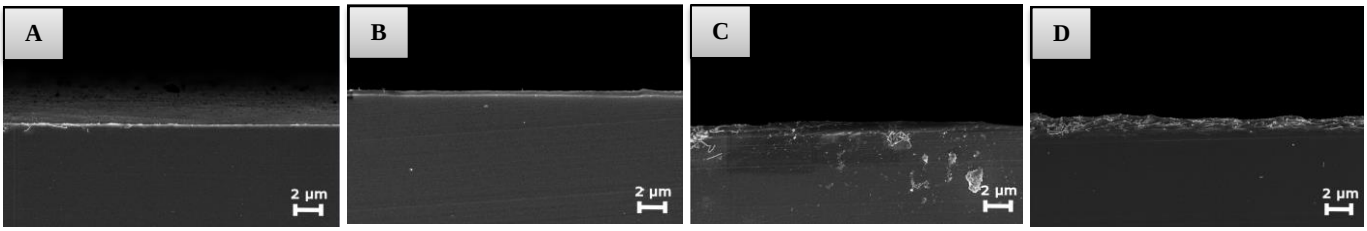

Figure 1: FEG-SEM cross section images of A) 12 µm wet estimated thickness coating B) 24 µm wet estimated thickness coating C) 40 µm wet estimated thickness coating D) 100 µm wet estimate thickness coating

The measured average thicknesses are respectively 217 ± 27, 349 ± 52, 851 ± 79 and 1733 ± 375 nm. A good linear correlation was found between wet and dry values (Figure 2**Error! Reference source not found.**A) proving a controlled thickness deposition and accurate measurement. Consequently, in this study the samples will be designated T-CNF/Ag NWs 200, T-CNF/Ag NWs 350, T-CNF/Ag NWs 850, T-CNF/Ag NWs 1750, referred according to their dry thickness.

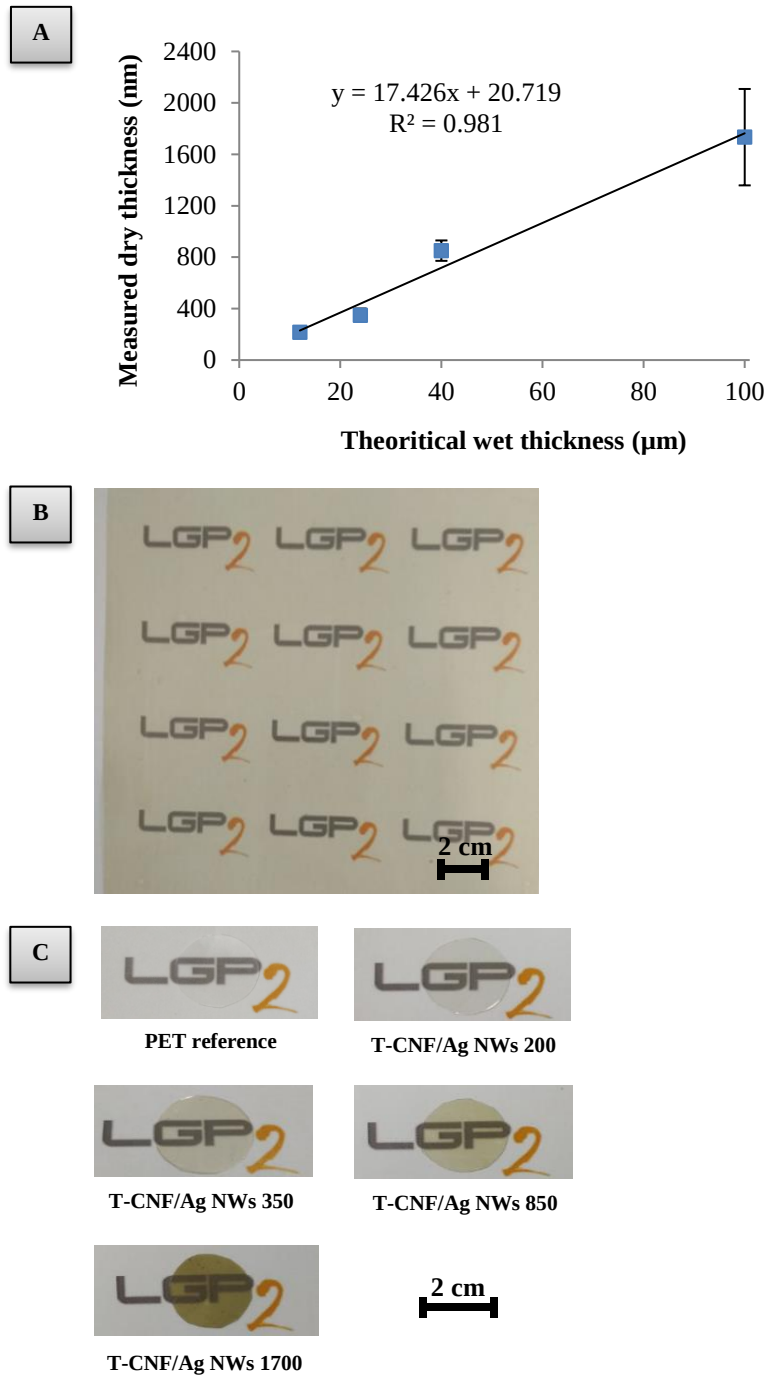

Figure 2: Coating quality investigated by A) measured dried thickness (nm) vs theoretical wet thickness (µm), B) qualitative picture of 15 cm x 15 cm large area of T-CNF/Ag NWs 350 sample and B) qualitative picture of reduced area of all produced samples (2 cm diameter) and scale bar.

From a macroscopic point of view, the coatings were observed to be uniform with no local uncoated patches (Figure 2B). For packaging applications, one of the key parameters for active coatings is to retain

transparency for the purpose of aesthetics and product display. The coatings were found to be relatively transparent as the LGP2 logo is clearly visible under the different samples displayed in Figure 2C. The transmittance at 550 nm was measured at 83.3, 75.6 and 67.3% respectively for T-CNF/Ag NWs 200, T-CNF/Ag NWs 350 and T-CNF/Ag NWs 850 samples, when compared to the 89.8% reference uncoated PET. Coating quality may also be determined by measuring conductivity (Fahad et al., 2019) and except for T-CNF/Ag NWs 200, the produced coatings display high conductivity (low sheet resistance) with a very low standard deviation, confirming coating uniformity (Figure 3B).

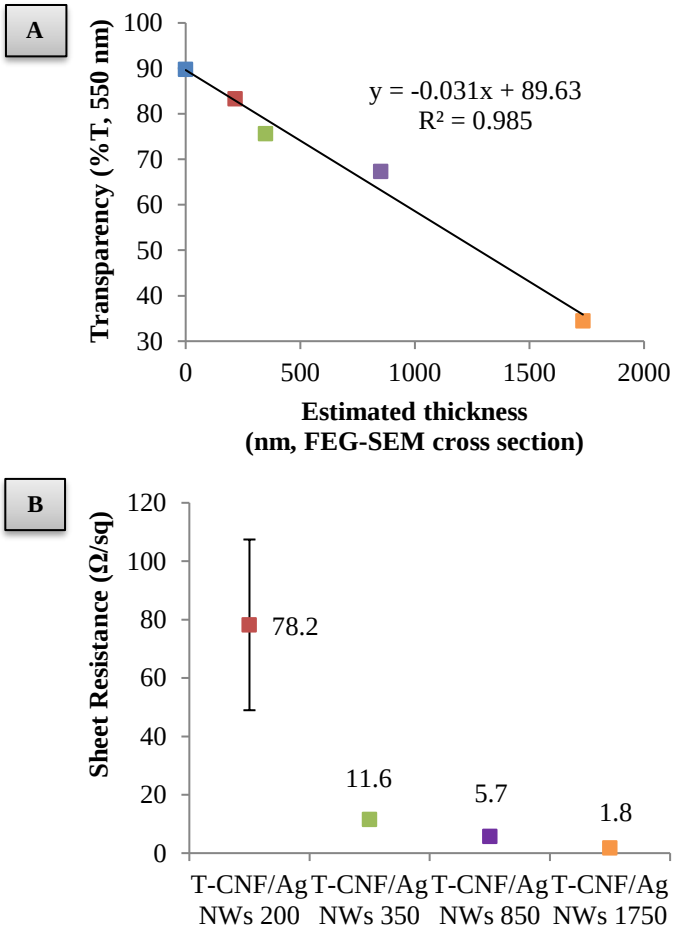

Figure 3: Coatings quality assessment using A) transparency measurement (%T, 550 nm) vs estimated dry thickness (nm) and B) sheet resistance measurements by 4-probe system (Ω /sq).

The morphology of the coated layer was also investigated using electron microscopy imaging (Figure 4) and the coated layer was found to be highly organized in a dense network, yet not aggregated, with an orientation of the Ag NWs toward the direction of shearing during the bar coating process.

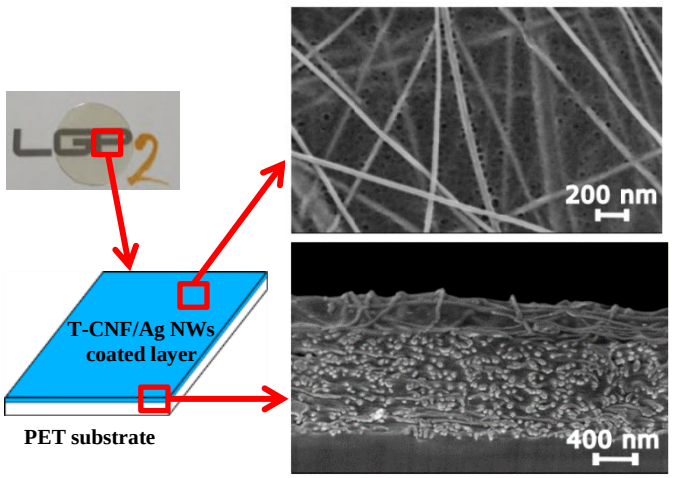

Figure 4: Schematic view of the T-CNF/Ag NWs 850 coated samples and FEG-SEM pictures of surface and cross-section

A preliminary leaching study was performed prior to antibacterial characterization. The test showed that no peaks corresponding to Ag NWs could be seen after recording UV-vis spectra of the recovered liquid media after the leaching assay (Supporting Information). It can then be concluded that there is only limited leaching of Ag NWs measured by this technique. The antibacterial activity of the active coatings was then investigated with qualitative inhibition zone test (Figure 5A). For the sample coated only with Ag NWs, a broad inhibition zone is visible proving the antibacterial activity of Ag NWs. The antibacterial activity of Ag NWs was established to be mainly due to the release of silver ions because of their lower surface area and thus lower adhesion with bacteria cell walls compared to spherical or cubic silver nanoparticles (Hong et al., 2016; Visnapuu et al., 2013). It can then be assumed that the broad inhibition zone of the sample is due to the release of silver ions into the media. For the sample coated with the mixture of both T-CNF and Ag NWs no inhibition zone can be seen which suggests that physically entrapping the Ag NWs within the T-CNF matrix leads to a contact killing mode of action with no or minimal release of active material.

To quantitatively verify the activity of the sample the AATCC standard method was performed against both Gram-positive *Staphylococcus Aureus* and Gram-negative *Escherichia Coli* (Figure 5B). The T-CNF/Ag NWs 200 sample show a surprising activity: it displays no impact against *E. Coli* whereas for *S. Aureus*, a strong reduction of 6.3 log of colony forming unit compared to the uncoated reference sample was noted, which corresponds to a 86.5% activity. Indeed, the bacterial activity in the presence of silver nanoparticles is usually higher for *E. Coli* than *S. Aureus* (Chernousova & Epple, 2013). This is explained by the difference in the bacteria cell wall: Gram-positive bacteria display a more permeable layer made of peptidoglycan only whereas Gram-negative bacteria have a thinner yet more impermeable lipopolysaccharide layer coupled to a thin peptidoglycan layer (Slavin et al., 2017). The difference in

activity observed when compared with the literature could be explained by the very thin coating layer for T-CNF/Ag NWs 200 which is probably close to the antibacterial activity limit of the coating. The T-CNF/Ag NWs 350 and T-CNF/Ag NWs 850 coatings displayed more or less the same performance respectively 89.3% *vs E.Coli*/100% *vs S. Aureus* and 87.6% *vs E.Coli*/100% *vs S. Aureus*, showing that a 350 nm thick coating is enough to achieve almost 100% antibacterial activity.

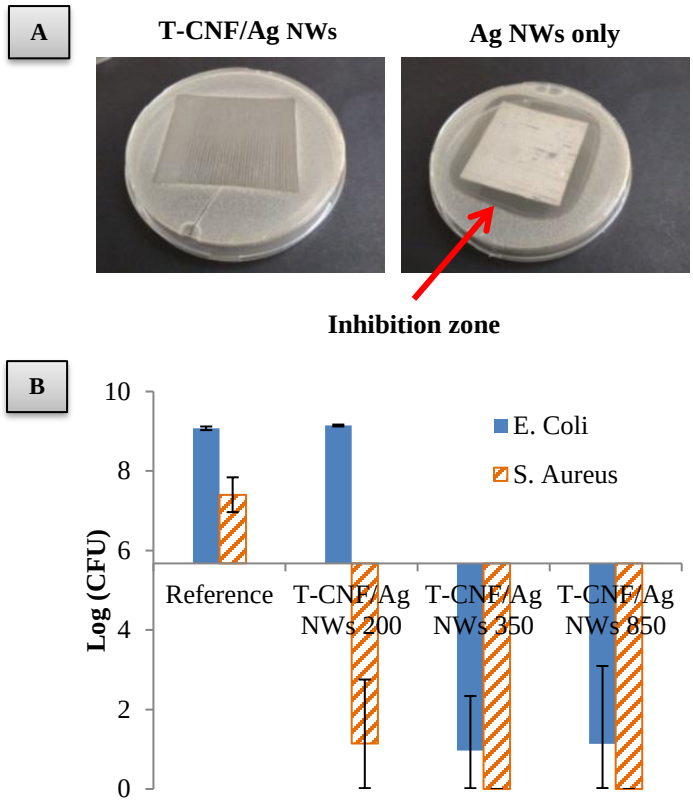

Figure 5: Antibacterial characterization of the coated samples by A) inhibition qualitative analysis for *E. Coli* bacteria strain B) qualitative analysis using AATCC standard method 100-1998 vs *E. Coli* and *S. Aureus* with results expressed in log of colony forming units (log CFU).

3.2. Bar coating on PLA and barrier properties.

In order to explore a bio-based substrate, the same ink was also deposited on polylactic acid (PLA) films using the bar coating process. The coatings were found to be homogeneous, with no uncoated patches and no visual defects (Figure 6A). The different deposited thickness for the PLA coatings were estimated to be relatively close to the ones for the PET coatings. Indeed the decrease of the transparency of the reference films due to the coating are more or less the same for both the PET and PLA coatings (Figure 6B). The

samples were then named with the same code, for instance T-CNF/Ag NWs 350 PLA corresponds to the T-CNF/Ag NWs coating on PLA with an approximated thickness of 350 nm.

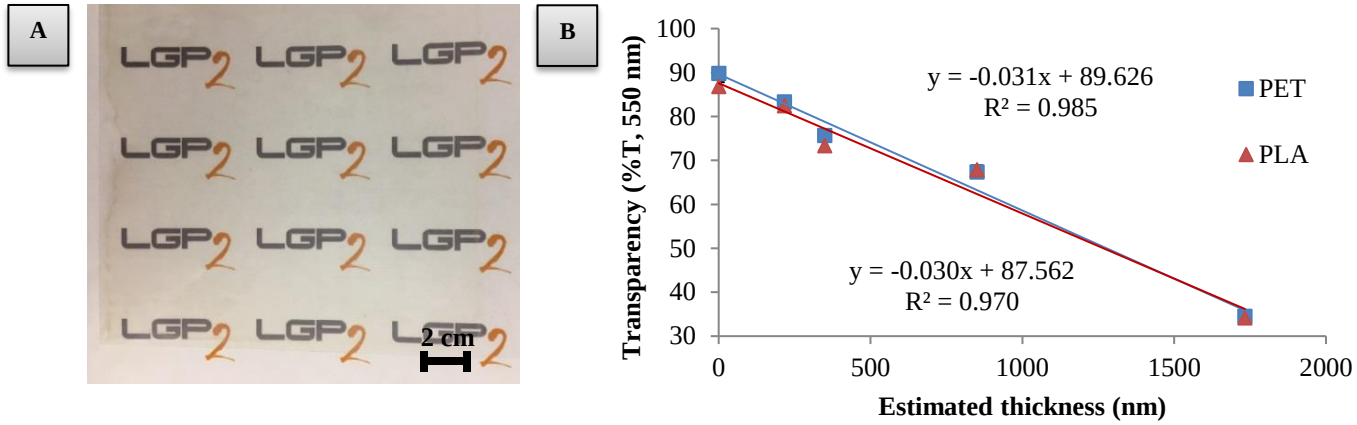

Figure 6: T-CNF/Ag NWs coating on PLA quality assessment with A) picture of 15 cm x 15 cm large area of T-CNF/Ag NWs 350 sample and B) transparency (%T, 550nm) measurements and comparison with coatings on PET.

CNF are often used in packaging application for their interesting barrier properties (Ferrer et al., 2017) and so the barrier properties of the coated PLA was investigated. Under dry conditions, the oxygen transmission rate (OTR) of the produced films was significantly decreased achieving more than 90% reduction for an estimated 1750 nm thick coatings (Figure 7A) but the measured values are however higher than those classically found in the literature for a T-CNF coating (Fukuzumi et al., 2009; Wu et al., 2017) (Figure 7A). Surprisingly in this study coating only T-CNF material was not possible due to high dewetting defect and so it was not possible to compare T-CNF/Ag NWs coatings to T-CNF coating only. A stronger surface treatment may be required to achieve T-CNF only coatings. CNF performance as a barrier layer is generally explained first by the large specific surface area and dense network of hydrogen bonding of the material which makes it difficult for any molecules to pass through (Ferrer et al., 2017). Then, CNF network also presents high tortuosity due to the impermeable crystalline regions and strong entanglement of the flexible fibres presenting a capability to seal any gaps within the network (Lagaron et al., 2004; Syverud & Stenius, 2008; Belbekhouche et al., 2011). Adding larger and rigid Ag NWs into the T-CNF matrix probably lead to a physical disruption of the sealed network and thus explaining the difference between the measured properties and the ones described in the literature.

As expected from using CNF materials, the OTR measurement is humidity dependent (Figure 7B) and at high humidity (80%) the OTR values of the different coatings are close to the uncoated PLA reference. The different coatings also showed a significant improvement of the WVTR values (Figure 7C) which is relatively similar (around 50% reduction) for all of the samples. This is interesting as coating CNF on polymer substrate usually leads to unchanged or slightly reduced water vapor permeability (Aulin et al.,

2013; Vartiainen et al., 2017), due to the hydrophilic nature and low water resistance of such materials. (Nair et al., 2014).

Coatings on biopolymer PLA sheets were successfully conducted and the coatings were found to be homogeneous with no uncoated patches and no visual defects. The deposited layers were found to be relatively similar to the coatings on PET and significant decrease for both the oxygen transmission rate and water vapour transmission rate was noted, proving the enhanced barrier properties.

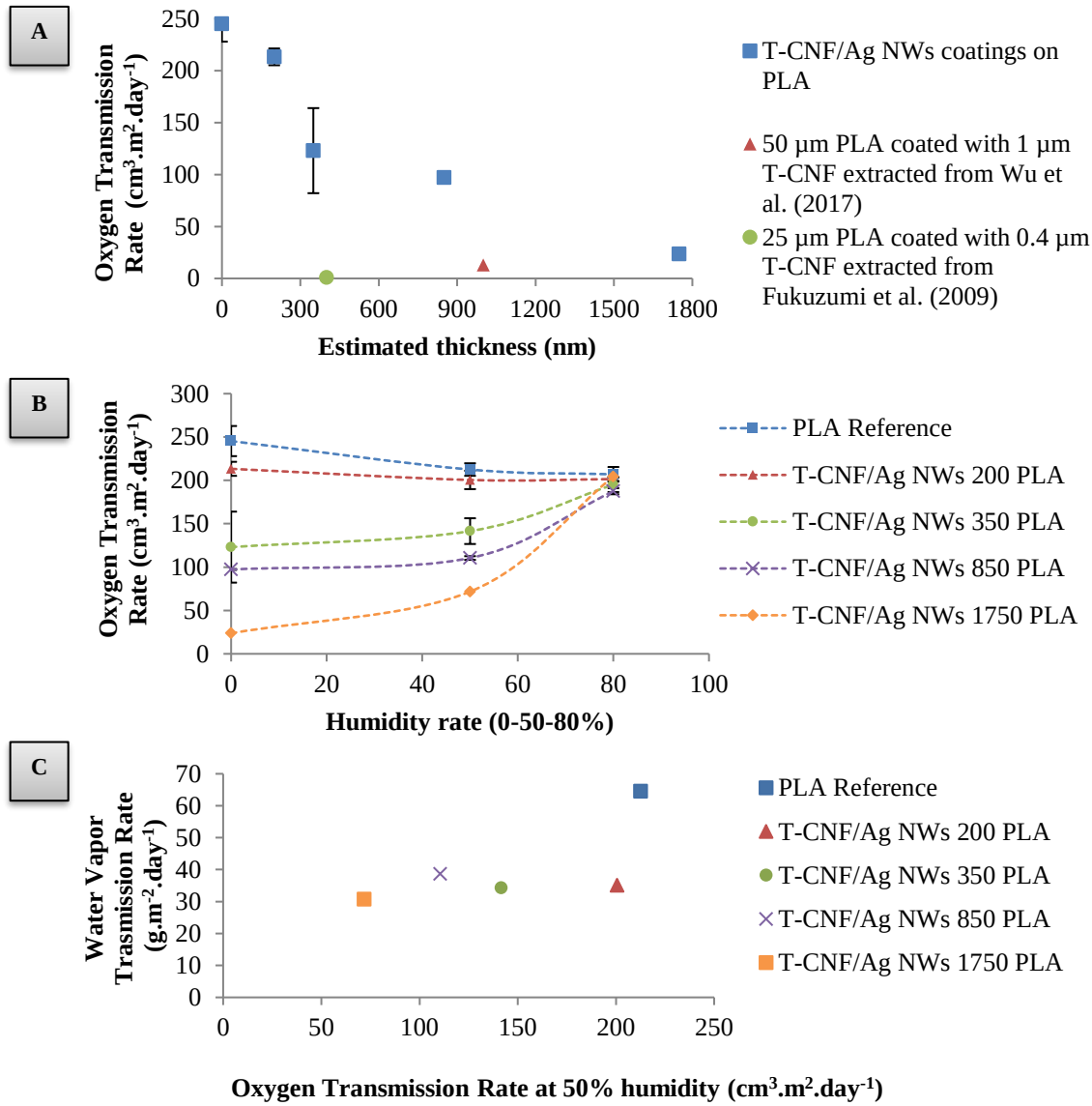

Figure 7: PLA coatings barrier properties characterizations with A) Oxygen Transmission Rate ($cm^3.m^{-2}.day^{-1}$) measurements in dry conditions vs estimated coating thickness (nm) and comparison with literature data B) Oxygen Transmission Rate ($cm^3.m^{-2}.day^{-1}$) measurements at different humidity rate (0-50-80%) and C) Water Vapor Transmission Rate ($g.m^{-2}.day^{-1}$) *vs* Oxygen Transmission Rate ($cm^3.m^{-2}.day^{-1}$) at 50% of humidity.

3.3. Up-scaling

As a more direct route and from a more economical point of view, a similar antibacterial ink was specifically formulated by simple mixing and redispersion of the separately supplied components T-CNF and Ag NWs in deionized water (see Materials and methods). The purchased T-CNF possess small dimensions (approximatively length 50-400 nm, diameter: 5-15 nm) and are rather rigid, as shown in the TEM images in Figure 8A. The silver nanowires dimensions were approximately one order of magnitude higher than the T-CNF: estimated length 10-50 µm, diameter 50-100 nm (Figure 8B and C).

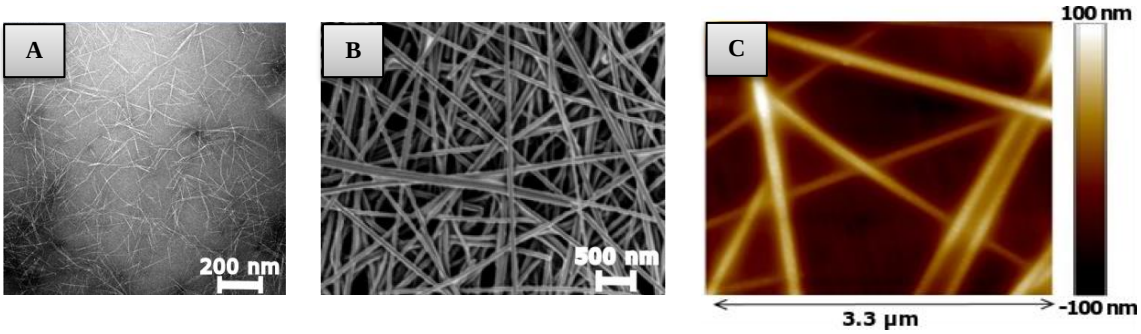

Figure 8: Raw materials microscopy imaging for A) TEM images of T-CNF B) SEM images of silver nanowires C) AFM images of silver nanowires

As it has already been described elsewhere (Hoeng et al., 2016), the T-CNF/Ag NWs ink is relatively stable over time and exhibits a very low sedimentation rate, for example 75% sedimentation height after 8 months of testing, as compared to the Ag NWs suspension without T-CNF, that sedimented completely after 4 days (Figure 9A). Flow curve rheology experiments were performed to assess the possibility to use coating process for ink deposition and both materials and the final formulation display classic strong shear thinning behaviour (Herrick et al., 1983; Hoeng et al., 2017) (Figure 9B). These behaviours can be explained by the high aspect ratio of the nanoparticles in these colloidal suspensions and the induced alignment of the particles at high shear rate, thus decreasing the viscosity. Ink viscosity at high shear rate was found to be in line with was expected for the bar coating process. It was found that for the different tested shear rate, viscosity of T-CNF suspension was one order of magnitude higher than Ag NWs. T-CNF dictates the viscosity in the T-CNF/Ag NWs ink by acting as a rheological modifier which was already shown in the literature for other aqueous CNF suspension coatings (Grüneberger et al., 2014).

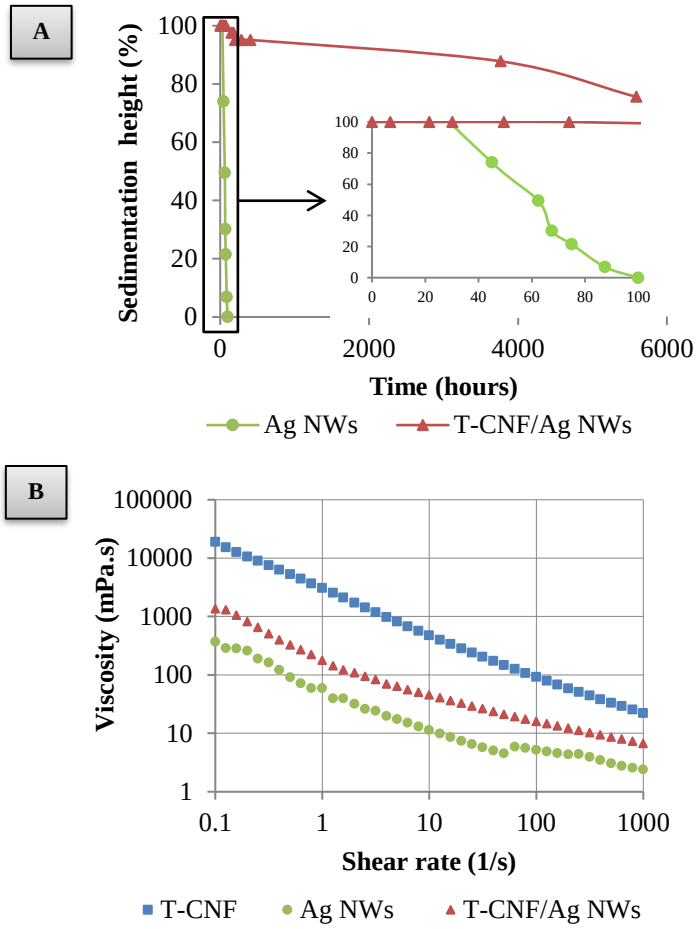

Figure 9: Ink formulation characterization compared to raw materials with A) sedimentation height measurement (%) and B) rheological flow curves. All formulations are at 1% wt total concentration.

3.3. Roll-to-roll process deposition

The potential for this formulation to be applied to industrial-like roll-to-roll coating process was also investigated using a reverse gravure coating process. Reverse gravure coating is interesting for packaging applications because of the wide range of inks and substrate that can be used and was also chosen because of the versatility of the process and the possibility to deposit low coat weights with a uniform and controlled thickness (Kipphan, 2001; Vak et al., 2016). Two different coating thicknesses were investigated and designated after their estimated wet thickness and previously established wet thickness/dry thickness relation for the bar-coated samples. In other words, T-CNF/Ag NWs 850RR for the coating using the roll 30 (wet coat thickness of 30-45 µm), and T-CNF/Ag NWs 200RR for the coating using roll 120 (wet coat thickness of 5-11 µm). The coatings were found to be visually of high quality with no uncoated patches, no visual defects and good homogeneity (Figure 10A). The antibacterial properties of the T-CNF/Ag NWs 200RR is relatively low whereas T-CNF/Ag NWs 850RR display a

strong antimicrobial effect (Figure 10B). The T-CNF/Ag NWs 850RR sample showed a strong and significant bactericidal effect, precisely 7.22 log reduction corresponding to 77.9% calculated antibacterial activity against *E. Coli* and 100% against *S. Aureus*. On the other hand, the T-CNF/Ag NWs 200RR sample showed no activity at all against *S. Aureus* whereas it showed a 7.57 log reduction corresponding to 81.7% activity against *E. Coli*. The measured antibacterial activity for the roll-to-roll coated samples using the up-scaled ink formulation were found to be in line with the results for the bar coated samples and thus the proposed solution for antibacterial packaging could hence be easily adapted to an industrial scale.

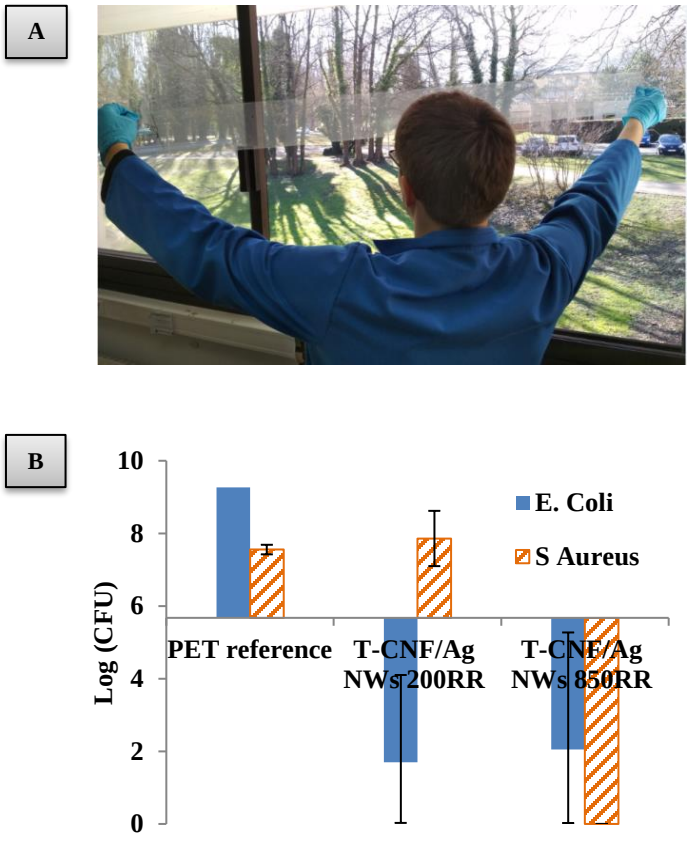

Figure 10: Roll-to-roll coatings with A) visual aspect of the coatings and B) AATCC qualitative method for antibacterial activity assessment.

4. Conclusion

An ink composed of silver nanowires and TEMPO-oxidised cellulose nanofibrils was successfully coated first on flexible and transparent polyethylene terephthalate sheets. The controlled thickness of the coatings ranged from 200 to 1750 nm with a high relative transparency superior to 65%, and the deposited layers were found to be homogeneous with no visual defects. The antibacterial activity was suggested to work by contact active killing mode of action and for the 350 nm thick coating, a significant AATCC standard antibacterial activity of 89.3% and 100% was noted respectively against Gram-negative *Escherichia Coli* and Gram-positive *Staphylococcus Aureus* bacteria. Moreover, the same ink was also deposited on PLA sheets with similar estimated thickness and quality. After coating, oxygen and water vapour permeability of the PLA substrate was significantly reduced, respectively 49% of oxygen transmission rate (dry conditions) and 47% reduction of water vapor transmission rate for 350 nm thick coating. Finally, a similar ink with lower cost materials was specifically formulated for up-scaling purposes and producing active surfaces using a roll-to-roll process was proved using the reverse gravure process, showing a strong retained antibacterial activity. Perspectives for a future work would be investigation of the migration of silver ions within the cellulose nanofibrils matrix and the influence of matrix surface chemistry and the investigation of the role of Ag NWs in the barrier properties of the system.

Declaration of competing interest

The authors declare that there is no conflict of interests with this manuscript.

Acknowledgements

This research was supported LabEx Tec 21 (Grant agreement No. ANR-11-LABX-0030). This research was made possible thanks to the facilities of the TekLiCell platform funded by the Région Rhône-Alpes (ERDF: European regional development fund). Authors want to thank Bertine Khelifi from Grenoble INP Pagora for the FEG-SEM imaging and Christine Lancelon-Pin from Cermav for the ultramicrotome cross-section preparation.

References

AATCC standard. (1998). *TM100 - Test Method for Antibacterial Finishes on Textile Materials: Assessment of Antibactrial Textile*. AATCC, Research Triangle Park, NC.

AFNOR standard. (2005). *NF EN 1104 - Papier et carton destinés à entrer en contact avec les denrées alimentaires : Détermination du transfert des constituants antimicrobiens*. AFNOR Association, La Plaine Saint-Denis, France.

Afra, E., Mohammadnejad, S., & Saraeyan, A. (2016). Cellulose nanofibils as coating material and its effects on paper properties. *Progress in Organic Coatings*, *101*, 455–460. https://doi.org/10.1016/J.PORGCOAT.2016.09.018

ASTM standard. (2014). *F1927, 14 - Test Method for Determination of Oxygen Gas Transmission Rate, Permeability and Permeance at Controlled Relative Humidity Through Barrier Materials Using a Coulometric Detector*. ASTM International, West Conshohocken PA.

Aulin, C., Karabulut, E., Tran, A., Wågberg, L., & Lindström, T. (2013). Transparent Nanocellulosic Multilayer Thin Films on Polylactic Acid with Tunable Gas Barrier Properties. *ACS Applied Materials & Interfaces*, *5*(15), 7352–7359. https://doi.org/10.1021/am401700n

Belbekhouche, S., Bras, J., Siqueira, G., Chappey, C., Lebrun, L., Khelifi, B., Marais, S., & Dufresne, A. (2011). Water sorption behavior and gas barrier properties of cellulose whiskers and microfibrils films. *Carbohydrate Polymers*, *83*(4), 1740–1748. https://doi.org/10.1016/j.carbpol.2010.10.036

Carlson, C., Hussain, S. M., Schrand, A. M., Braydich-Stolle, L. K., Hess, K. L., Jones, R. L., & Schlager, J. J. (2008). Unique cellular interaction of silver nanoparticles: size-dependent generation of reactive oxygen species. *The Journal of Physical Chemistry. B*, *112*(43), 13608–13619. https://doi.org/10.1021/jp712087m

Chernousova, S., & Epple, M. (2013). Silver as Antibacterial Agent: Ion, Nanoparticle, and Metal. *Angewandte Chemie International Edition*, *52*(6), 1636–1653. https://doi.org/10.1002/anie.201205923

El Badawy, A. M., Silva, R. G., Morris, B., Scheckel, K. G., Suidan, M. T., & Tolaymat, T. M. (2011). Surface Charge-Dependent Toxicity of Silver Nanoparticles. *Environmental Science & Technology*, *45*(1), 283–287. https://doi.org/10.1021/es1034188

Fahad, S., Yu, H., Wang, L., Zain-ul-Abdin, Haroon, M., Ullah, R. S., Nazir, A., Naveed, K.-R., Elshaarani, T., & Khan, A. (2019). Recent progress in the synthesis of silver nanowires and their role as conducting materials. *Journal of Materials Science*, *54*(2), 997–1035. https://doi.org/10.1007/s10853-018-2994-9

Ferrer, A., Pal, L., & Hubbe, M. (2017). Nanocellulose in packaging: Advances in barrier layer technologies. *Industrial Crops and Products*, *95*(Supplement C), 574–582. https://doi.org/10.1016/j.indcrop.2016.11.012

Food and Agriculture Organization of the United Nations. (2019). *World food and agriculture: statistical pocketbook 2019*.

Fukuzumi, H., Saito, T., Iwata, T., Kumamoto, Y., & Isogai, A. (2009). Transparent and High Gas Barrier Films of Cellulose Nanofibers Prepared by TEMPO-Mediated Oxidation. *Biomacromolecules*, *10*(1), 162–165. https://doi.org/10.1021/bm801065u

Grüneberger, F., Künniger, T., Zimmermann, T., & Arnold, M. (2014). Rheology of nanofibrillated cellulose/acrylate systems for coating applications. *Cellulose*, *21*(3), 1313–1326. https://doi.org/10.1007/s10570-014-0248-9

Herrick, F. W., Casebier, R. L., Hamilton, J. K., & Sandberg, K. R. (1983). Microfibrillated Cellulose: Morphology and Accessibility. *J. Appl. Polym. Sci.: Appl. Polym. Symp.; (United States)*, *37*. https://www.osti.gov/scitech/biblio/5039044

Hoeng, F., Denneulin, A., Krosnicki, G., & Bras, J. (2016). Positive impact of cellulose nanofibrils on silver nanowire coatings for transparent conductive films. *Journal of Materials Chemistry C*, *4*(46), 10945–10954. https://doi.org/10.1039/C6TC03629E

Hoeng, F., Denneulin, A., Reverdy-Bruas, N., Krosnicki, G., & Bras, J. (2017). Rheology of cellulose nanofibrils/silver nanowires suspension for the production of transparent and conductive electrodes by screen printing. *Applied Surface Science*, *394*(Supplement C), 160–168. https://doi.org/10.1016/j.apsusc.2016.10.073

Hong, X., Wen, J., Xiong, X., & Hu, Y. (2016). Shape effect on the antibacterial activity of silver nanoparticles synthesized via a microwave-assisted method. *Environmental Science and Pollution Research*, *23*(5), 4489–4497. https://doi.org/10.1007/s11356-015-5668-z

Ilić, V., Šaponjić, Z., Vodnik, V., Potkonjak, B., Jovančić, P., Nedeljković, J., & Radetić, M. (2009). The influence of silver content on antimicrobial activity and color of cotton fabrics functionalized with Ag nanoparticles. *Carbohydrate Polymers*, *78*(3), 564–569. https://doi.org/10.1016/j.carbpol.2009.05.015

Kaur, R., & Liu, S. (2016). Antibacterial surface design – Contact kill. *Progress in Surface Science*, *91*(3), 136–153. https://doi.org/10.1016/j.progsurf.2016.09.001

Kipphan, H. (Ed.). (2001). *Handbook of Print Media: Technologies and Production Methods*. Springer-Verlag. https://doi.org/10.1007/978-3-540-29900-4

Korani, M., Ghazizadeh, E., Korani, S., Hami, Z., & Mohammadi-Bardbori, A. (2015). Effects of silver nanoparticles on human health. *European Journal of Nanomedicine*, *7*(1), 51–62. https://doi.org/10.1515/ejnm-2014-0032

Kvítek, L., Panáček, A., Soukupová, J., Kolář, M., Večeřová, R., Prucek, R., Holecová, M., & Zbořil, R. (2008). Effect of Surfactants and Polymers on Stability and Antibacterial Activity of Silver Nanoparticles (NPs). *The Journal of Physical Chemistry C*, *112*(15), 5825–5834. https://doi.org/10.1021/jp711616v

Lagaron, J. M., Catalá, R., & Gavara, R. (2004). Structural characteristics defining high barrier properties in polymeric materials. *Materials Science and Technology*, *20*(1), 1–7. https://doi.org/10.1179/026708304225010442

Martins, N. C. T., Freire, C. S. R., Pinto, R. J. B., Fernandes, S. C. M., Neto, C. P., Silvestre, A. J. D., Causio, J., Baldi, G., Sadocco, P., & Trindade, T. (2012). Electrostatic assembly of Ag nanoparticles onto nanofibrillated cellulose for antibacterial paper products. *Cellulose*, *19*(4), 1425–1436. https://doi.org/10.1007/s10570-012-9713-5

Morones, J. R., Elechiguerra, J. L., Camacho, A., Holt, K., Kouri, J. B., Ramírez, J. T., & Yacaman, M. J. (2005). The bactericidal effect of silver nanoparticles. *Nanotechnology*, *16*(10), 2346. https://doi.org/10.1088/0957-4484/16/10/059

Nair, S. S., Zhu, J., Deng, Y., & Ragauskas, A. J. (2014). High performance green barriers based on nanocellulose. *Sustainable Chemical Processes*, *2*, 23. https://doi.org/10.1186/s40508-014-0023-0

Pal, S., Tak, Y. K., & Song, J. M. (2007). Does the Antibacterial Activity of Silver Nanoparticles Depend on the Shape of the Nanoparticle? A Study of the Gram-Negative Bacterium Escherichia coli. *Applied and Environmental Microbiology*, *73*(6), 1712–1720. https://doi.org/10.1128/AEM.02218-06

582 Rai, M. k., Deshmukh, S. d., Ingle, A. p., & Gade, A. k. (2012). Silver nanoparticles: the powerful
583 nanoweapon against multidrug-resistant bacteria. *Journal of Applied Microbiology*, *112*(5), 841–
584 852. https://doi.org/10.1111/j.1365-2672.2012.05253.x
585 Ramaraju, B., Imae, T., & Destaye, A. G. (2015). Ag nanoparticle-immobilized cellulose nanofibril films
586 for environmental conservation. *Applied Catalysis A: General*, *492*(Supplement C), 184–189.
587 https://doi.org/10.1016/j.apcata.2014.12.045
588 Rodionova, G., Saito, T., Lenes, M., Eriksen, Ø., Gregersen, Ø., Fukuzumi, H., & Isogai, A. (2012).
589 Mechanical and oxygen barrier properties of films prepared from fibrillated dispersions of
590 TEMPO-oxidized Norway spruce and Eucalyptus pulps. *Cellulose*, *19*(3), 705–711.
591 https://doi.org/10.1007/s10570-012-9664-x
592 Schindelin, J., Arganda-Carreras, I., Frise, E., Kaynig, V., Longair, M., Pietzsch, T., Preibisch, S.,
593 Rueden, C., Saalfeld, S., Schmid, B., Tinevez, J.-Y., White, D. J., Hartenstein, V., Eliceiri, K.,
594 Tomancak, P., & Cardona, A. (2012). Fiji: an open-source platform for biological-image analysis.
595 *Nature Methods*, *9*(7), 676–682. https://doi.org/10.1038/nmeth.2019
596 Schneider, C. A., Rasband, W. S., & Eliceiri, K. W. (2012). NIH Image to ImageJ: 25 years of image
597 analysis. *Nature Methods*, *9*(7), 671–675. https://doi.org/10.1038/nmeth.2089
598 Slavin, Y. N., Asnis, J., Häfeli, U. O., & Bach, H. (2017). Metal nanoparticles: understanding the
599 mechanisms behind antibacterial activity. *Journal of Nanobiotechnology*, *15*(1), 65.
600 https://doi.org/10.1186/s12951-017-0308-z
601 Smetana, A. B., Klabunde, K. J., Marchin, G. R., & Sorensen, C. M. (2008). Biocidal Activity of
602 Nanocrystalline Silver Powders and Particles. *Langmuir*, *24*(14), 7457–7464.
603 https://doi.org/10.1021/la800091y
604 Sofi, S. A., Singh, J., Rafiq, S., Ashraf, U., Dar, B. N., & Nayik, G. A. (2018). A Comprehensive Review
605 on Antimicrobial Packaging and its Use in Food Packaging. *Current Nutrition & Food Science*,
606 *14*(4), 305–312. https://doi.org/10.2174/1573401313666170609095732
607 Syverud, K., & Stenius, P. (2008). Strength and barrier properties of MFC films. *Cellulose*, *16*(1), 75.
608 https://doi.org/10.1007/s10570-008-9244-2
609 TAPPI Standard. (2009). *T 448 om-09 - Water vapor transmission rate of paper and paperboard at 23°C*
610 *and 50% RH*. Technical Association of the Pulp and Paper Industry, New York.
611 Turbak, A. F., Snyder, F. W., & Sandberg, K. R. (1983). Microfibrillated Cellulose, a New Cellulose
612 Product: Properties, Uses, and Commercial Potential. *J. Appl. Polym. Sci.: Appl. Polym. Symp.;*
613 *(United States)*, *37*. https://www.osti.gov/scitech/biblio/5062478
614 Uddin, K. M. A., Orelma, H., Mohammadi, P., Borghei, M., Laine, J., Linder, M., & Rojas, O. J. (2017).
615 Retention of lysozyme activity by physical immobilization in nanocellulose aerogels and
616 antibacterial effects. *Cellulose*, *24*(7), 2837–2848. https://doi.org/10.1007/s10570-017-1311-0
617 Vak, D., Weerasinghe, H., Ramamurthy, J., Subbiah, J., Brown, M., & Jones, D. J. (2016). Reverse
618 gravure coating for roll-to-roll production of organic photovoltaics. *Solar Energy Materials and*
619 *Solar Cells*, *149*, 154–161. https://doi.org/10.1016/j.solmat.2016.01.015
620 Vartiainen, J., Laine, C., Willberg-Keyriläinen, P., Pitkänen, M., & Ohra-aho, T. (2017). Biobased
621 mineral-oil barrier-coated food-packaging films. *Journal of Applied Polymer Science*, *134*(9).
622 https://doi.org/10.1002/app.44586
623 Visnapuu, M., Joost, U., Juganson, K., Künnis-Beres, K., Kahru, A., Kisand, V., & Ivask, A. (2013).
624 Dissolution of Silver Nanowires and Nanospheres Dictates Their Toxicity to Escherichia coli.
625 *BioMed Research International*, *2013*, 1–9. https://doi.org/10.1155/2013/819252

626 Wu, B., Geng, B., Chen, Y., Liu, H., Li, G., & Wu, Q. (2017). Preparation and characteristics of TEMPO-
627 oxidized cellulose nanofibrils from bamboo pulp and their oxygen-barrier application in PLA
628 films. *Frontiers of Chemical Science and Engineering*, *11*(4), 554–563.
629 https://doi.org/10.1007/s11705-017-1673-8
630 Xu, Y., Li, S., Yue, X., & Lu, W. (2017). Review of Silver Nanoparticles (AgNPs)-Cellulose Antibacterial
631 Composites. *BioResources*, *13*(1), 2150-2170–2170. https://doi.org/10.15376/biores.13.1.Xu
632 Yildirim, S., Röcker, B., Pettersen, M. K., Nilsen-Nygaard, J., Ayhan, Z., Rutkaite, R., Radusin, T.,
633 Suminska, P., Marcos, B., & Coma, V. (2018). Active Packaging Applications for Food.
634 *Comprehensive Reviews in Food Science and Food Safety*, *17*(1), 165–199.
635 https://doi.org/10.1111/1541-4337.12322
636 Yu, Z., Wang, W., Kong, F., Lin, M., & Mustapha, A. (2019). Cellulose nanofibril/silver nanoparticle
637 composite as an active food packaging system and its toxicity to human colon cells. *International*
638 *Journal of Biological Macromolecules*, *129*, 887–894.
639 https://doi.org/10.1016/j.ijbiomac.2019.02.084